Nanoscale

PAPER

Cite this: *Nanoscale*, 2019, **11**, 13961

Dose-dependent effect of proton irradiation on electrical properties of WSe_2 ambipolar field effect transistors†

Jiwon Shin,[a] Kyungjune Cho,[a] Tae-Young Kim,‡[a] Jinsu Pak,[a] Jae-Keun Kim,[a] Woocheol Lee,[a] Jaeyoung Kim,[a] Seungjun Chung,[b] Woong-Ki Hong *[c] and Takhee Lee *[a]

The irradiation effect of high energy proton beams on tungsten diselenide (WSe_2) ambipolar field-effect transistors was investigated. We measured the electrical characteristics of the fabricated WSe_2 FETs before and after the 10 MeV proton beam irradiation with different doses of 10^{12}, 10^{13}, 10^{14}, and 10^{15} cm^{-2}. For low dose conditions (10^{12}, 10^{13}, and 10^{14} cm^{-2}), the threshold voltages shifted to the negative gate voltage direction, and the current in the hole and electron accumulation regimes decreased and increased, respectively. However, the trends were opposite for the high dose condition (10^{15} cm^{-2}); the threshold voltages shifted to the positive gate voltage direction, and the current in the hole and electron accumulation regimes increased and decreased, respectively. These phenomena can be explained by the combined effect of proton irradiation-induced traps and the applied gate bias condition. Specifically, irradiation-induced positive oxide traps in SiO_2 dielectrics play a role in enhancing electron accumulation and reducing hole accumulation in the WSe_2 channel, whereas the irradiation-induced holes near the WSe_2/SiO_2 interface act as electron trapping sites, with enhancing hole accumulation and reducing electron accumulation in the WSe_2 channel. This work will help improve the understanding of the effect of high energy irradiation on WSe_2-based and other ambipolar nanoelectronic devices. In addition, this work shows the possibility of tuning the electrical properties of WSe_2-based devices.

Received 19th April 2019,
Accepted 22nd June 2019

DOI: 10.1039/c9nr03345a

rsc.li/nanoscale

Introduction

Two-dimensional (2D) semiconducting transition-metal dichalcogenides (TMDs) have gained significant attention due to their unique electronic and optoelectronic properties, the presence of energy band gaps from the visible and near infrared spectral ranges, and atomically thin film structures.[1–6] To date, tremendous efforts have been devoted to designing and synthesizing 2D TMDs and to exploring their potential applications.[2,7–14] Therefore, understanding the fundamental mechanisms and controlling the properties of 2D TMDs are crucial for further versatile applications in integrated devices including energy systems, light emitting devices, field effect transistors (FETs) and photodetectors.[3,5,6,10,15–19]

The material properties of 2D TMDs can be effectively tuned through various methods such as dimension reduction, heterostructure formation, intercalation, doping, strain engineering, and especially the irradiation effects of ions or electrons.[3,13,19–31] In particular, most irradiation studies to date have been focused on single type charge carriers in TMD devices.[29–31] Among 2D TMDs, tungsten diselenide (WSe_2) has recently been studied from the perspective of irradiation effects of ion- and electron-beams.[32–35] WSe_2 has many excellent properties, such as a tunable bandgap (1.2–1.67 eV), ambipolar transport behaviour, and weak or nonexistent Fermi level pinning at metal-WSe_2 interfaces;[3,25,36] these properties make 2D WSe_2 a promising candidate for potential device applications, including valley-based electronics, spin-electronics, and optoelectronics.[23,37–39] To the best of our knowledge, there is no report on the electrical transport properties of WSe_2 FETs showing p-type and n-type conduction through irradiation of high energy proton beams.

In this work, we studied the effect of high energy proton beam irradiation on the ambipolar WSe_2 FETs. The devices

[a]*Department of Physics and Astronomy, and Institute of Applied Physics, Seoul National University, Seoul 08826, Korea. E-mail: tlee@snu.ac.kr*
[b]*Photo-Electronic Hybrids Research Center, Korea Institute of Science and Technology, Seoul 02792, Korea*
[c]*Jeonju Center, Korea Basic Science Institute, Jeonju, Jeollabuk-do 54907, Korea. E-mail: wkh27@kbsi.re.kr*

† Electronic supplementary information (ESI) available. See DOI: 10.1039/c9nr03345a

‡ Present address: Flash Process Architecture Team, Samsung Electronics, 114, Samseong-ro, Pyeongtaek-si, Gyeonggi-do 17786, Korea.

were irradiated with 10 MeV energy protons under different dose conditions of 10^{12}, 10^{13}, 10^{14} and 10^{15} cm^{-2}. The electrical characteristics of the WSe_2 FETs such as the current level and threshold voltages were measured before and after the proton beam irradiation, and the changes after the irradiation were analysed statistically. Additionally, we measured physicochemical properties such as lattice vibration, binding energy, and thickness of the WSe_2 flakes using Raman spectra, AFM images, and X-ray photoelectron spectra. After the proton beam irradiation, the electrical properties were changed due to the irradiation-induced traps from the substrate, not from WSe_2 itself.

Results and discussion

The WSe_2 FETs were fabricated with mechanically exfoliated WSe_2 flakes on heavily p-doped Si substrates with a 270 nm-thick SiO_2 dielectric layer. Fig. 1a shows the optical image of a transferred WSe_2 flake on the Si/SiO_2 substrate. The WSe_2 flake shown in Fig. 1a was found to be ~4 nm-thick using an atomic force microscope (AFM) (Fig. 1b). Fig. 1c shows the optical image of a WSe_2-based device made with the flake shown in Fig. 1a and b. The electrical properties of the fabricated WSe_2 FET were examined, as shown in Fig. 1d–f. Transfer characteristics (drain–source current *versus* gate voltage, I_{DS}–V_{GS}) (Fig. 1d) and output characteristics (drain–source current *versus* drain–source voltage, I_{DS}–V_{DS}) (Fig. 1e and f) show a sharp increase of I_{DS} at both negative (the hole accumulation regime, marked by blue colour) and positive (the electron accumulation regime, marked by red colour) gate voltages, indicating the gate-induced charge injection from metal/WSe_2 contacts. According to Podzorov *et al.*,[40] the Schottky-type FETs exhibit ambipolar characteristics by gate-controlled tunneling of injected charges (hole and electron) through the Schottky barriers formed at the metal/WSe_2 semiconductor contacts. The electrical properties of other ambipolar WSe_2 FETs can be found in the ESI (Fig. S2).†

After electrical characterization of the fabricated WSe_2 FETs, the devices were subsequently irradiated by proton beams of 10 MeV for 10, 100, 1000, and 10 000 seconds, corresponding to dose values of ~10^{12}, 10^{13}, 10^{14}, and 10^{15} cm^{-2}, respectively. The electrical characteristics of WSe_2 FETs were measured and compared before and after proton beam irradiation, as shown in Fig. 2 (see Fig. S3a in the ESI†). In the transfer curves of the device recorded at fixed V_{DS} = 1 V, both

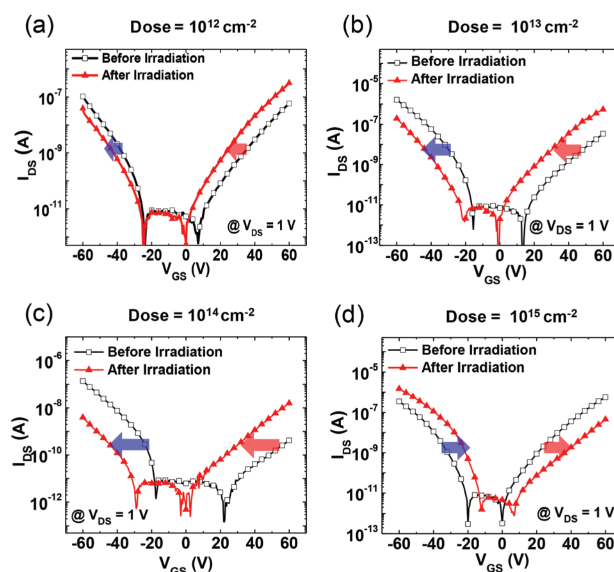

Fig. 2 Transfer curves of the WSe_2 FETs before and after proton beam irradiation under the doses of (a) 10^{12}, (b) 10^{13}, (c) 10^{14}, and (d) 10^{15} cm^{-2}.

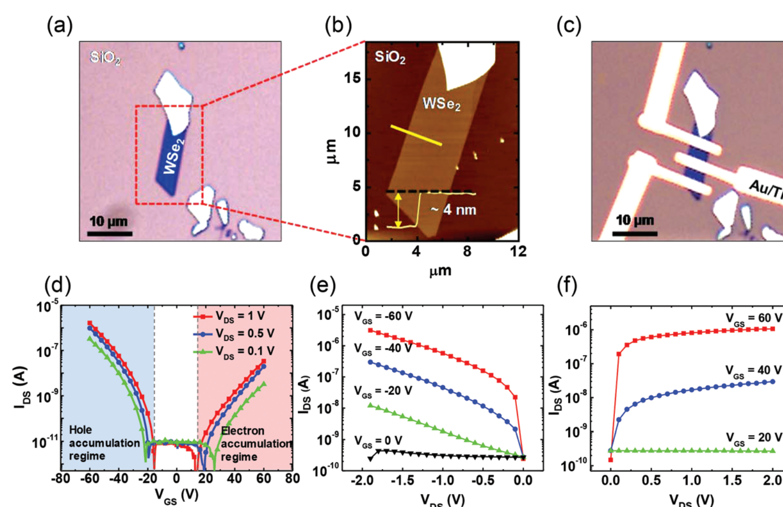

Fig. 1 (a) An optical image of a multilayer WSe_2 flake. (b) An AFM image of the selected region in (a) with a cross-sectional profile across a line in the image. (c) An optical image of the fabricated FET using this WSe_2 flake. (d) The transfer curves of the fabricated WSe_2 FET recorded at V_{DS} = 0.1 V, 0.5 V, and 1 V. The output curves for (e) negative gate voltages and (f) positive gate voltages recorded at different gate voltages.

This journal is © The Royal Society of Chemistry 2019

the threshold voltages for hole and electron accumulation regimes shifted to the negative gate voltage direction after the proton beam irradiation for the doses of ~10^{12}, 10^{13}, and 10^{14} cm^{-2} (Fig. 2a–c). The drain–source current level of the hole accumulation regime decreased, whereas that of the electron accumulation regime increased. For example, after the proton beam irradiation under a 10^{12} cm^{-2} dose, the drain–source current decreased from 0.11 μA to 0.04 μA at V_{DS} = 1 V and V_{GS} = −60 V for the hole accumulation regime, and it increased from 0.06 μA to 0.31 μA at V_{DS} = 1 V and V_{GS} = 60 V for the electron accumulation regime (Fig. 2a). Under the low irradiation dose conditions of ~10^{12}, 10^{13}, and 10^{14} cm^{-2}, the shifted amount of the threshold voltage seemed to increase as the dose increased (marked by blue and red arrows in Fig. 2a–c). Correspondingly, the amount of current change in the hole and electron accumulation regimes became larger as the dose increased (Fig. 2a–c). For example, after the proton beam irradiation under a 10^{14} cm^{-2} dose, the drain–source current decreased from 140 nA to 4 nA at V_{DS} = 1 V and V_{GS} = −60 V for the hole accumulation regime, and it increased from 0.4 nA to 16 nA at V_{DS} = 1 V and V_{GS} = 60 V for the electron accumulation regime (Fig. 2c). However, the WSe_2 FETs that were irradiated with a proton beam dose of 10^{15} cm^{-2} showed different behaviour compared to the devices irradiated under low dose conditions (Fig. 2d). After proton beam irradiation under a 10^{15} cm^{-2} dose, the threshold voltages shifted to the positive gate voltage direction for both hole and electron accumulation regimes, and the drain–source current increased in the hole accumulation regime while it decreased in the electron accumulation regime. These dose-dependent phenomena of proton beam irradiation will be explained in detail later in terms of the combined effects by irradiation-induced charges and gate-bias conditions.

To clarify these different trends between the two cases of low and high proton beam doses, we statistically investigated the changes of current and threshold voltage as a function of proton beam dose. We measured a total of 20 devices, with 4–6 devices for each proton beam irradiation condition. Fig. 3a and b summarize the changes of threshold voltages for the WSe_2 FETs after the proton beam irradiation under dose conditions of 10^{12}, 10^{13}, 10^{14}, and 10^{15} cm^{-2} for hole and electron accumulation regimes at V_{DS} = 1 V, respectively. Note that the threshold voltage was determined by the value of the *x*-intercept of the tangent line from the point that has the maximum differential value in the transfer curve. In Fig. 3a and b, similar to Fig. 2, the threshold voltages for both hole and electron accumulation regimes moved to the negative gate voltage direction for low dose conditions of ~10^{12}, 10^{13}, and 10^{14} cm^{-2}. In addition, as the irradiation dose increased, the threshold voltages shifted more. However, the threshold voltage of the devices irradiated with a high dose proton beam (10^{15} cm^{-2}) shifted to the positive gate voltage direction. Fig. 3c and d summarize the changes of the device current after the proton beam irradiation for hole and electron accumulation regimes, respectively. The currents shown in Fig. 3c and d are the values measured at V_{DS} = 1 V with V_{GS} = −60 V for the hole accumulation regime and V_{GS} = 60 V for the electron accumulation regime. The device current for the hole accumulation regime (Fig. 3c) decreased as the irradiation dose increased to 10^{14} cm^{-2}, and then it increased at a dose of 10^{15} cm^{-2}. The current showed an opposite tendency for the electron accumulation regime (Fig. 3d); the current increased as the irradiation dose increased to 10^{14} cm^{-2}, and then it decreased at a dose of 10^{15} cm^{-2}. As we mentioned above, these results can be explained by the irradiation-induced positive oxide traps in the gate dielectric SiO_2 layer and electron trapping at the interface between SiO_2 and WSe_2. Note that mobility and subthreshold swing values are also summarized as a function of proton dose (see Fig. S4 and S5 of the ESI†), but they did not show a clear trend with the dose conditions as the threshold voltages or currents did.

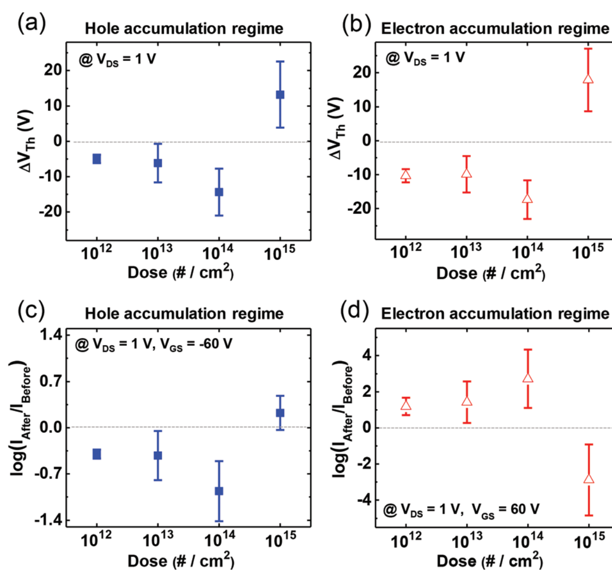

Fig. 3 Threshold voltage shift measured at V_{DS} = 1 V as a function of proton irradiation dose condition for the (a) hole accumulation regime and (b) electron accumulation regime. The normalized I_{DS} (current ratio before and after irradiation, I_{after}/I_{before}) measured at V_{DS} = 1 V as a function of proton irradiation dose condition for the (c) hole accumulation regime and (d) electron accumulation regime.

To verify whether such variations of electrical characteristics are caused by proton beam-irradiated WSe_2 flakes themselves, we examined the structural characteristics, elemental composition, and electronic state of WSe_2 flakes before and after the proton beam irradiation by Raman spectroscopy and X-ray photoemission spectroscopy (XPS). Fig. 4 shows the measured results for a high dose condition of 10^{15} cm^{-2}. Raman mapping data of the WSe_2 flake (Fig. 4a and b) show no noticeable differences before and after proton beam irradiation. Specifically, in Raman spectra (Fig. 4c), the position and intensity of three prominent Raman peaks corresponding to the lattice vibration mode of $E^1{}_{2g}$ (254 cm^{-1}), A_{1g} (254 cm^{-1} and 264 cm^{-1}), and $B^1{}_{2g}$ (310 cm^{-1})[38,41,42] were not noticeably changed after proton beam irradiation. The XPS result (Fig. 4d) shows three dominant binding energy peaks of

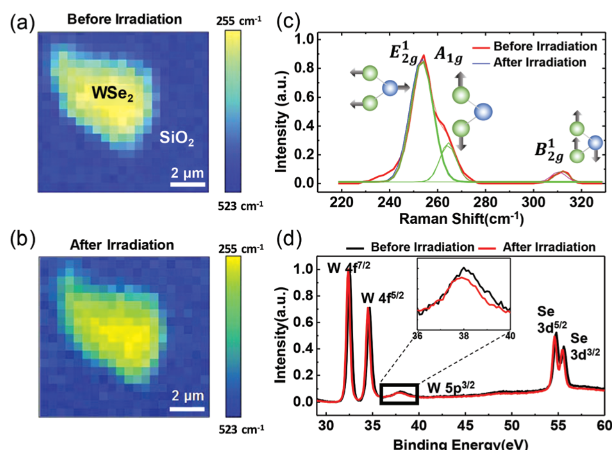

Fig. 4 (a and b) Raman mapping, (c) Raman spectra, and (d) XPS spectra of WSe_2 flakes before and after proton irradiation at a dose of 10^{15} cm^{-2}.

tungsten and two dominant peaks of selenium.[42,43] These five peaks did not show a considerable change after proton beam irradiation. Note that a little redshift (by ~0.1 eV) was observed after proton beam irradiation (Fig. 4d), which may have originated from a dipole effect due to the irradiation-induced electron trapping at the interface between SiO_2 and WSe_2 with a van der Waals gap.[44–46] As a result, the physicochemical characteristics of WSe_2 were not damaged by proton beam irradiation, and therefore, the change of the electrical characteristics after proton beam irradiation is not considered to be caused by the WSe_2 itself.

The experimental results can be explained by the combined effects of the proton beam irradiation-induced traps and the applied gate bias condition. When high-energy protons are irradiated on the WSe_2 FETs, protons generate various kinds of traps. The high energy protons slow down mainly by an electronic stopping process, generating electron–hole pairs. After the protons sufficiently slow down, they lose the majority of the energy by a nuclear stopping process, and then they stop near the stopping depth and damage the lattice around the stopping depth.[47–49] To calculate the stopping depth, we simulated energy-loss profiles using Stopping and Range of Ions in Matter (SRIM) software. According to the SRIM results, most of the protons would stop near 700 μm from the surface (Fig. S6 in the ESI†). Since the thickness of the device is approximately 500 μm (4–7 nm for the WSe_2 flake, 270 nm for the SiO_2 layer, and 500 μm for the Si layer), most of the protons would penetrate through the entire device structure and electron–hole pairs are generated along the paths. The SiO_2 layer is the most sensitive to the ionization process. After electron–hole pairs are generated, they recombine for a few picoseconds, but some of the holes remained near the generated location while electrons are swept away much faster.[50,51] The trapped holes in the SiO_2 layer (denoted as "positive oxide traps") cause the modulation of gate electric field, resulting in the depletion effect of holes and enhancement effect of electrons in the WSe_2 channel (Fig. 5a and c). Some of the generated holes undergo anomalous stochastic hopping transport through the SiO_2 layer and reach the WSe_2/SiO_2 interface under the high dose conditions (Fig. 5e and g). These holes that reach the interface can cause the formation of a layer of electron trapping sites, resulting in the enhancement effect of holes and depletion effect of electrons in the WSe_2 channel (Fig. 5e and g). As a result, positive oxide traps play a role in enhancing electron accumulation and reducing hole accumulation in the WSe_2 channel, whereas the electron trapping sites near the WSe_2/SiO_2 interface (denoted as "interface electron trap sites") enhance hole accumulation in the WSe_2 channel. Because the interface electron trap sites require a longer proton irradiation time than the positive oxide traps, the effect of the positive oxide traps in SiO_2 bulk is more influential for low dose conditions (10^{12}, 10^{13}, and 10^{14} cm^{-2}) (Fig. 5a–d). In the energy band diagrams, due to the positive oxide traps, electrons are efficiently injected into the WSe_2 channel under positively

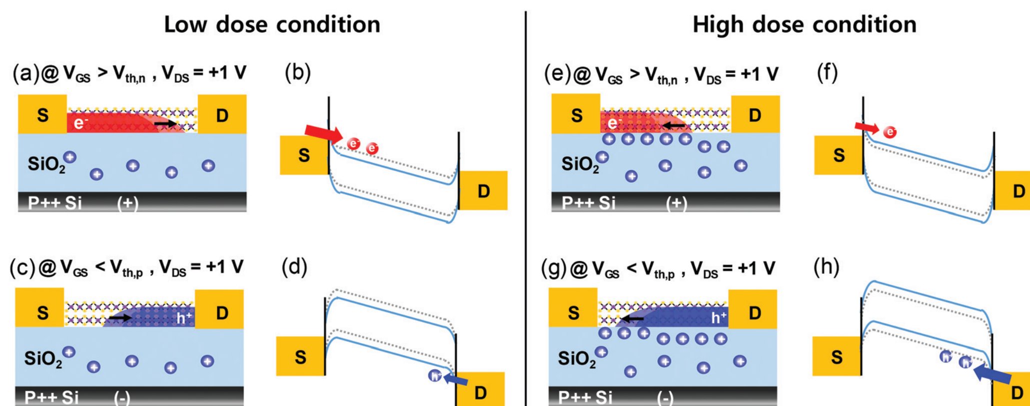

Fig. 5 Schematic illustrations of the device structure and energy band diagrams depicting the conduction mechanism after proton beam irradiation. For low dose conditions (10^{12}, 10^{13}, and 10^{14} cm^{-2}), the effect of positive oxide traps is dominant, resulting in the enhancement of electron accumulation in the channel (a–d). For the high dose condition (10^{15} cm^{-2}), the effect of interface electron trap sites is dominant, resulting in the enhancement of hole accumulation in the channel (e–h).

 This journal is © The Royal Society of Chemistry 2019

applied gate voltage (Fig. 5b) while it becomes difficult to inject holes into the WSe_2 channel under negatively applied gate voltage (Fig. 5d). Thus, the threshold voltage shifts to the negative gate voltage direction (Fig. 2a–c, 3a and b). As the proton beam irradiation dose increases, more positive oxide traps are generated. Therefore, the threshold voltage shift can be larger because the positive oxide traps increase as the proton beam irradiation dose increases, as shown in Fig. 3a and b. However, under a high dose condition of 10^{15} cm^{-2}, the effect of interface electron trap sites becomes dominant, and therefore, the threshold voltage shifts to the positive gate voltage direction (Fig. 2d, 3a and b). Here, it becomes difficult to inject electrons into the WSe_2 channel (Fig. 5f) and easier to inject holes into the WSe_2 channel (Fig. 5h).

Conclusions

We investigated the irradiation effect of a high-energy (10 MeV) proton beam on the WSe_2 FETs with ambipolar characteristics. The electrical properties such as the current and threshold voltages of the WSe_2 devices were changed after proton beam irradiation, depending on the beam dose conditions due to the combining effect of the proton beam irradiation-induced charges and applied gate bias. Under low dose conditions (10^{12}, 10^{13}, and 10^{14} cm^{-2}), the positive trapped holes in the SiO_2 dielectric layer cause the modulation of effective gate field on electron and hole accumulation in the WSe_2 channel, resulting in a threshold voltage shift towards the negative gate voltage direction. Under the high dose condition (10^{15} cm^{-2}), the irradiation-induced holes near the WSe_2/SiO_2 interface act as electron-trapped sites and enhance hole accumulation in the WSe_2 channel, resulting in a threshold voltage shift towards the positive gate voltage direction. This study may provide a method to control the electrical properties of WSe_2 FETs through proton beam irradiation. Furthermore, this study may contribute to a deeper understanding of the influence of high-energy proton beams on ambipolar WSe_2-based nanoelectronic devices and be helpful for the application of TMD-based devices in harsh radiation environments such as space.

Experimental section

Fabrication of WSe_2 FETs

WSe_2 flakes were exfoliated by the mechanical exfoliation method from a bulk WSe_2 crystal (purchased from HQ Graphene). The WSe_2 flakes were transferred onto a SiO_2 (270 nm)/Si (500 μm) substrate. The Si substrate that was heavily boron doped can be used as a bottom gate with a resistivity 5×10^{-3} Ω cm^{-1}. The thicknesses of WSe_2 flakes were measured with an AFM (NX 10 AFM, Park Systems) and the WSe_2 flakes with the thickness in the 4–7 nm range were used to fabricate ambipolar FETs (Fig. S8†). The source and drain electrodes were patterned by electron-beam lithography (JSM-6510, JEOL). PMMA 950 K A5 (5% concentration in anisole) and MMA (8.5) MAA (9% concentration in ethyl lactate) were spin-coated as bilayer electron beam resists. Then, Ti (5 nm)/Au (40 nm) was sequentially deposited as the source and drain electrodes by electron-beam evaporation.

Electrical and optical characterization

The electrical characteristics of the fabricated devices were measured in a probe station (ST-500, JANIS) using a semi-conductor parameter analyzer (Keithley 4200 SCS) under vacuum (~10^{-4} Torr). Raman spectra of WSe_2 flakes were recorded by using a Raman spectrometer (XperRam 200, Nanobase, Inc.) with a 532 nm laser as the excitation source. The laser power was 40 μW with a diffraction-limited laser spot size of ~1 μm. The XPS spectra were measured by electron spectroscopy for chemical analysis (AXIS SUPRA) at the National Center for Inter-university Research Facilities.

Proton beam irradiation

The fabricated devices were exposed to proton beams with different dose conditions of 10^{12}, 10^{13}, 10^{14}, and 10^{15} cm^{-2}. The proton beam facility used for this research was the MC-50 cyclotron at the Korea Institute of Radiological and Medical Sciences. The proton beam had an energy of 10 MeV with an average current 10 nA, corresponding to irradiated 6.25×10^{10} protons per seconds. All the measurements for the proton-irradiated devices were performed one day after the proton irradiation since the radioactivity had to fall below the safe level.

Conflicts of interest

There are no conflicts to declare.

Acknowledgements

The authors appreciate the financial support from the National Creative Research Laboratory program (Grant No. 2012026372) through the National Research Foundation of Korea (NRF), funded by the Korean Ministry of Science and ICT. W. K. H acknowledges the financial support from the Korea Basic Science Institute (KBSI) (Grant No. C38521). We are especially thankful for the beam time grants from the proton beam facilities of the Korea Institute of Radiological and Medical Sciences.

Notes and references

1 K. F. Mak, C. Lee, J. Hone, J. Shan and T. F. Heinz, Atomically Thin MoS_2: A New Direct-Gap Semiconductor, *Phys. Rev. Lett.*, 2010, **105**, 136805.
2 Q. H. Wang, K. Kalantar-Zadeh, A. Kis, J. N. Coleman and M. S. Strano, Electronics and Optoelectronics of Two-

Dimensional Transition Metal Dichalcogenides, *Nat. Mater.*, 2012, **7**, 699–712.
3 H. Wang, H. Yuan, S. S. Hong, Y. Li and Y. Cui, Physical and Chemical Tuning of Two-Dimensional Transition Metal Dichalcogenides, *Chem. Soc. Rev.*, 2015, **44**, 2664–2680.
4 B. Radisavljevic, A. Radenovic, J. Brivio, V. Giacometti and A. Kis, Single-Layer MoS_2 Transistors, *Nat. Nanotechnol.*, 2011, **6**, 147–150.
5 K. F. Mak and J. Shan, Photonics and Optoelectronics of 2D Semiconductor Transition Metal Dichalcogenides, *Nat. Photonics*, 2016, **10**, 216–226.
6 J. Y. Lee, J.-H. Shin, G.-H. Lee and C. H. Lee, Two-Dimensional Semiconductor Optoelectronics Based on van der Waals Heterostructures, *Nanomaterials*, 2016, **6**, 193.
7 T. Mueller and E. Malic, Exciton Physics and Device Application of Two-Dimensional Transition Metal Dichalcogenide Semiconductors, *npj 2D Mater. Appl.*, 2018, **2**, 29.
8 R. Lv, J. A. Robinson, R. E. Schaak, D. Sun, Y. Sun, T. E. Mallouk and M. J. Terrones, Transition Metal Dichalcogenides and Beyond: Synthesis, Properties, and Applications of Single-and Few-Layer Nanosheets, *Acc. Chem. Res.*, 2014, **48**, 56–64.
9 N. Choudhary, M. R. Islam, N. Kang, L. Tetard, Y. Jung and S. I. Khondaker, Two-Dimensional Lateral Heterojunction through Bandgap Engineering of MoS_2 via Oxygen Plasma, *J. Phys.: Condens. Matter*, 2016, **28**, 364002.
10 W. Huh, S. Jang, J. Y. Lee, D. Lee, D. Lee, J. M. Lee, H.-G. Park, J. C. Kim, H. Y. Jeong, G. Wang and C.-H. Lee, Synaptic Barristor Based on Phase-Engineered 2D Heterostructures, *Adv. Mater.*, 2018, **30**, 1801447.
11 X. Liu, I. Balla, H. Bergeron, G. P. Campbell, M. J. Bedzyk and M. C. Hersam, Rotationally Commensurate Growth of MoS_2 on Epitaxial Graphene, *ACS Nano*, 2016, **10**, 1067–1075.
12 I. S. Kim, V. K. Sangwan, D. Jariwala, J. D. Wood, S. Park, K.-S. Chen, F. Shi, F. Ruiz-Zepeda, A. Ponce, M. Jose-Yacaman, V. P. Dravid, T. J. Marks, M. C. Hersam and L. J. Lauhon, Influence of Stoichiometry on the Optical and Electrical Properties of Chemical Vapor Deposition Derived MoS_2, *ACS Nano*, 2014, **8**, 10551–10558.
13 D. Jariwala, S. L. Howell, K.-S. Chen, J. Kang, V. K. Sangwan, S. A. Filippone, R. Turrisi, T. J. Marks, L. J. Lauhon and M. C. Hersam, Hybrid, Gate-Tunable, van der Waals p–n Heterojunctions from Pentacene and MoS_2, *Nano Lett.*, 2016, **16**, 497–503.
14 H. Bergeron, V. K. Sangwan, J. J. McMorrow, G. P. Campbell, I. Balla, X. Liu, M. J. Bedzyk, T. J. Marks and M. C. Hersam, Chemical Vapor Deposition of Monolayer MoS_2 Directly on Ultrathin Al_2O_3 for Low-Power Electronics, *Appl. Phys. Lett.*, 2017, **110**, 053101.
15 W. Choi, N. Choudhary, G. H. Han, J. Park, D. Akinwande and Y. H. Lee, Recent Development of Two-Dimensional Transition Metal Dichalcogenides and Their Applications, *Mater. Today*, 2017, **20**, 116–130.
16 A. Pospischil, M. M. Furchi and T. Mueller, Solar-Energy Conversion and Light Emission in an Atomic Monolayer p–n Diode, *Nat. Nanotechnol.*, 2014, **9**, 257–261.
17 S. S. Varghese, S. H. Varghese, S. Swaminathan, K. K. Singh and V. Mittal, Two-Dimensional Materials for Sensing: Graphene and Beyond, *Electronics*, 2015, **4**, 651–687.
18 K. Cho, M. Min, T.-Y. Kim, H. Jeong, J. Pak, J.-K. Kim, J. Jang, S. J. Yun, Y. H. Lee, W.-K. Hong and T. Lee, Electrical and Optical Characterization of MoS_2 with Sulfur Vacancy Passivation by Treatment with Alkanethiol Molecules, *ACS Nano*, 2015, **9**, 8044–8053.
19 C.-J. Park, H. J. Park, J. Y. Lee, J. Kim, C.-H. Lee and J. Joo, Photovoltaic Field-Effect Transistors Using a MoS_2 and Organic Rubrene van der Waals Hybrid, *ACS Appl. Mater. Interfaces*, 2018, **10**, 29848–29856.
20 R. Zhang, D. Drysdale, V. Koutsos and R. Cheung, Controlled Layer Thinning and p-Type Doping of WSe_2 by Vapor XeF_2, *Adv. Funct. Mater.*, 2017, **27**, 1702455.
21 J. Lee, J. Huang, B. G. Sumpter and M. Yoon, Strain-Engineered Optoelectronic Properties of 2D Transition Metal Dichalcogenide Lateral Heterostructures, *2D Mater.*, 2017, **4**, 021016.
22 W. S. Yun, S. W. Han, S. C. Hong, I. G. Kim and J. D. Lee, Thickness and Strain Effects on Electronic Structures of Transition Metal Dichalcogenides: 2H-MX_2 Semiconductors (M = Mo, W; X = S, Se, Te), *Phys. Rev. B: Condens. Matter Mater. Phys.*, 2012, **85**, 033305.
23 C. Zhou, Y. Zhao, S. Raju, Y. Wang, Z. Lin, M. Chan and Y. Chai, Carrier Type Control of WSe_2 Field-Effect Transistors by Thickness Modulation and MoO_3 Layer Doping, *Adv. Funct. Mater.*, 2016, **26**, 4223–4230.
24 D. Kiriya, M. Tosun, P. Zhao, J. S. Kang and A. Javey, Air-Stable Surface Charge Transfer Doping of MoS_2 by Benzyl Viologen, *J. Am. Chem. Soc.*, 2014, **136**, 7853–7856.
25 P. R. Pudasaini, A. Oyedele, C. Zhang, M. G. Stanford, N. Cross, A. T. Wong, A. N. Hoffman, K. Xiao, G. Duscher, D. G. Mandrus, T. Z. Ward and P. D. Rack, High-Performance Multilayer WSe_2 Field-Effect Transistors with Carrier Type Control, *Nano Res.*, 2018, **11**, 722–730.
26 N. Huo, S. Tongay, W. Guo, R. Li, C. Fan, F. Lu, J. Yang, B. Li, Y. Li and Z. Wei, Novel Optical and Electrical Transport Properties in Atomically Thin WSe_2/MoS_2 p–n Heterostructures, *Adv. Electron. Mater.*, 2015, **1**, 1400066.
27 X. Cui, G.-H. Lee, Y. D. Kim, G. Arefe, P. Y. Huang, C.-H. Lee, D. A. Chenet, X. Zhang, L. Wang, F. Ye, F. Pizzocchero, B. S. Jessen, K. Watanabe, T. Taniguchi, D. A. Muller, T. Low, P. Kim and J. Hone, Multi-Terminal Transport Measurements of MoS_2 Using a van der Waals Heterostructure Device Platform, *Nat. Nanotechnol.*, 2015, **10**, 534–540.
28 R. C. Walker, T. Shi, E. C. Silva, I. Jovanovic and J. A. Robinson, Radiation Effects on Two-Dimensional Materials, *Phys. Status Solidi A*, 2016, **213**, 3065–3077.
29 T.-Y. Kim, K. Cho, W. Park, J. Park, Y. Song, S. Hong, W.-K. Hong and T. Lee, Irradiation Effects of High-Energy Proton Beams on MoS_2 Field Effect Transistors, *ACS Nano*, 2014, **8**, 2774–2781.

 This journal is © The Royal Society of Chemistry 2019

30 F. Giubileo, L. Iemmo, M. Passacantando, F. Urban, G. Luongo, L. Sun, G. Amato, E. Enrico and A. Di Bartolomeo, Effect of Electron Irradiation on the Transport and Field Emission Properties of Few-Layer MoS_2 Field-Effect Transistors, *J. Phys. Chem. C*, 2018, **123**, 1454–1461.
31 S. Bertolazzi, S. Bonacchi, G. Nan, A. Pershin, D. Beljonne and P. Samorì, Engineering Chemically Active Defects in Monolayer MoS_2 Transistors via Ion-Beam Irradiation and Their Healing via Vapor Deposition of Alkanethiols, *Adv. Mater.*, 2017, **29**, 1606760.
32 M. G. Stanford, P. R. Pudasaini, A. Belianinov, N. Cross, J. H. Noh, M. R. Koehler, D. G. Mandrus, G. Duscher, A. J. Rondinone and I. N. Ivanov, Focused Helium-Ion Beam Irradiation Effects on Electrical Transport Properties of Few-Layer WSe_2: Enabling Nanoscale Direct Write Homo-Junctions, *Sci. Rep.*, 2016, **6**, 27276.
33 D. Kim, H. Du, T. Kim, S. Shin, S. Kim, M. Song, C. Lee, J. Lee, H. Cheong, D. H. Seo and S. Seo, The Enhanced Low Resistance Contacts and Boosted Mobility in Two-Dimensional p-type WSe_2 Transistors through Ar^+ Ion-Beam Generated Surface Defects, *AIP Adv.*, 2016, **6**, 105307.
34 T. Shi, R. C. Walker, I. Jovanovic and J. A. Robinson, Effects of Energetic Ion Irradiation on WSe_2/SiC Heterostructures, *Sci. Rep.*, 2017, **7**, 4151.
35 G. Moody, K. Tran, X. Lu, T. Autry, J. M. Fraser, R. P. Mirin, L. Yang, X. Li and K. L. Silverman, Microsecond Valley Lifetime of Defect-Bound Excitons in Monolayer WSe_2, *Phys. Rev. Lett.*, 2018, **121**, 057403.
36 S. Das and J. Appenzeller, WSe_2 Field Effect Transistors with Enhanced Ambipolar Characteristics, *Appl. Phys. Lett.*, 2013, **103**, 103501.
37 Z. Wang, Q. Li, Y. Chen, B. Cui, Y. Li, F. Besenbacher and M. Dong, The Ambipolar Transport Behavior of WSe_2 Transistors and its Analogue Circuits, *NPG Asia Mater.*, 2018, **10**, 703–712.
38 W. Zhao, Z. Ghorannevis, K. K. Amara, J. R. Pang, M. Toh, X. Zhang, C. Kloc, P. H. Tan and G. Eda, Lattice Dynamics in Mono- and Few-Layer Sheets of WS_2 and WSe_2, *Nanoscale*, 2013, **5**, 9677–9683.
39 A. Ramasubramaniam, Large Excitonic Effects in Monolayers of Molybdenum and Tungsten Dichalcogenides, *Phys. Rev. B: Condens. Matter Mater. Phys.*, 2012, **86**, 115409.
40 V. Podzorov, M. E. Gershenson, C. Kloc, R. Zeis and E. Bucher, High-Mobility Field-Effect Transistors based on Transition Metal Dichalcogenides, *Appl. Phys. Lett.*, 2004, **84**, 3301–3303.
41 P. Tonndorf, R. Schmidt, P. Böttger, X. Zhang, J. Börner, A. Liebig, M. Albrecht, C. Kloc, O. Gordan, D. R. Zahn, S. M. de Vasconcellos and R. Bratschitsch, Photoluminescence Emission and Raman Response of Monolayer MoS_2, $MoSe_2$, and WSe_2, *Opt. Express*, 2013, **21**, 4908–4916.
42 J. Huang, L. Yang, D. Liu, J. Chen, Q. Fu, Y. Xiong, F. Lin and B. Xiang, Large-Area Synthesis of Monolayer WSe_2 on a SiO_2/Si Substrate and its Device Applications, *Nanoscale*, 2015, **7**, 4193–4198.
43 G. Salitra, G. Hodes, E. Klein and R. Tenne, Highly Oriented WSe_2 Thin Films Prepared by Selenization of Evaporated WO_3, *Thin Solid Films*, 1994, **245**, 180–185.
44 H. Fang, C. Battaglia, C. Carraro, S. Nemsak, B. Ozdol, J. S. Kang, H. A. Bechtel, S. B. Desai, F. Kronast, A. A. Unal, G. Conti, C. Conlon, G. K. Palsson, M. C. Martin, A. M. Minor, C. S. Fadley, E. Yablonovitch, R. Maboudian and A. Javey, Strong Interlayer Coupling in van der Waals Heterostructures Built from Single-Layer Chalcogenides, *Proc. Natl. Acad. Sci. U. S. A.*, 2014, **111**, 6198–6202.
45 T. C. Taucher, I. Hehn, O. T. Hofmann, M. Zharnikov and E. Zojer, Understanding Chemical versus Electrostatic Shifts in X-Ray Photoelectron Spectra of Organic Self-Assembled Monolayers, *J. Phys. Chem. C*, 2016, **120**, 3428–3437.
46 L. Q. Zhu, K. Kita, T. Nishimura, K. Nagashio, S. K. Wang and A. Toriumi, Interfacial Dipole at High-k Dielectric/SiO_2 Interface: X-Ray Photoelectron Spectroscopy Characteristics, *Jpn. J. Appl. Phys.*, 2011, **50**, 031502.
47 C. Claeys and E. Simoen, *Radiation Effects in Advanced Semiconductor Materials and Devices*, Springer, Berlin, 2013.
48 S. R. Messenger, E. A. Burke, G. P. Summers, M. A. Xapsos, R. J. Walters, E. M. Jackson and B. D. Weaver, Nonionizing Energy Loss (NIEL) for Heavy Ions, *IEEE Trans. Nucl. Sci.*, 1999, **46**, 1595–1602.
49 J. F. Ziegler, J. P. Biersack and U. Littmark, *The Stopping and Range of Ions in Matter*, Pergamon, New York, 1985.
50 R. C. Hughes, Charge-Carrier Transport Phenomena in Amorphous SiO_2: Direct Measurement of the Drift Mobility and Lifetime, *Phys. Rev. Lett.*, 1973, **30**, 1333.
51 T. R. Oldham, *Ionizing Radiation Effects in MOS Oxides*, World Scientific, Singapore, 1999.

This journal is © The Royal Society of Chemistry 2019